Modeling and Control of Active Gravity Off-Loading for Deployable Space Structures

Trevor J. Bihl[*a], Khanh D. Pham[b], Thomas W. Murphey[b]
[a]Ohio University, School of Electrical Engineering and Computer Science, 286 Stocker Center, Athens, OH, USA 45701-2979;
[b]Air Force Research Laboratory, Space Vehicles Directorate, 3550 Aberdeen Ave. SE, Kirtland AFB, NM USA 87117-5776

ABSTRACT

The mechanics of deployable space structures are examined through ground based testing to predict the structures' deployment in a microgravity environment. In order to simulate the microgravity conditions a test article would experience in space, a method of counteracting the loads and deflections induced by gravity is required. This is accomplished through various gravity off-loading methods, which introduce forces opposite and equal to the force of gravity acting upon a test article throughout its deployment. Current gravity off-loading methods are passive rail-cart systems with their movement forced due to their physical coupling with a test article; this introduces unwanted boundary conditions, such as inertia and side-loading from a test article's transverse movement. Therefore, an active gravity off-loading method is being developed that will deploy simultaneously with a test article. This method employs motorized carts with active position control based upon the lead angle of the off-loading cable. The maximum allowable lead angle is designed to be ±5°, with the intention of minimizing the forcing of the carts' longitudinal deployment. System dynamics and kinematics analytical modeling is derived. Simulated system results from the analytical system model and preliminary results from the prototype are presented.

Keywords: Gravity off-loading, gravity compensation, deployable structures, control systems

1. INTRODUCTION

Ground testing is required to estimate the reliability of all equipment to be used in space. In testing deployable space structures, it is important to account for many structures being designed to meet the minimum strength and stiffness required of them in a microgravity environment; hence they can be unable to adequately support their own weight in a 1-g environment [1], [2]. For accurate ground testing of deployable space structures, a gravity off-loaded test environment that introduces a force equal and opposite to the gravitational force is required. The presence of an inadequately compensated gravitational force can alter the deployment characteristics during a test, as modal analysis of a test article can be overly corrupted from mass loading of over 5% of a test article mass [3].

Currently, gravity off-loaded testing is accomplished through a variety of passive and active methods. Passive methods used in practice include balloons [3], neutral buoyancy simulation [4] and carts on a rail, which suspend a test article with counterweights. However, many of these methods cannot be employed without introducing mass loading to a test article, potentially corrupting the results of an experiment [3]. For example, passive carts on a rail can introduce many unwanted affects, such as oscillations induced by a test article's deployment dynamics, cart static friction or counterweight oscillations. Additionally, inertia equal to twice a test article's mass can be added by the counterweight if there is any vertical deployment.

Active methods, such as magnetic pneumatic suspension devices [3], can be used for accurate 1 degree of freedom (DOF) testing. Typically these methods would not introduce a mass loading force of over 5% [3], and therefore potentially avoid corrupting the modal analysis of a test deployment. However, there are size

[*] Trevor.J.Bihl.1@ohio.edu; phone 1 740 981-6210; fax 1 740 593-0778; ohio.edu

Sensors and Systems for Space Applications, edited by Richard T. Howard, Robert D. Richards
Proc. of SPIE Vol. 6555, 655515, (2007) · 0277-786X/07/$18 · doi: 10.1117/12.717410

and power requirements with magnetic-pneumatic suspension devices that make them difficult to use in testing structures such as trusses and booms that can deploy both horizontally and vertically.

Given the limitations of currently available systems, an accurate active gravity off-loading system that supports 2 DOF testing is desirable. At the Air Force Research Laboratory's Space Vehicles Directorate (AFRL/VS), such a system is currently under development and is currently in the prototyping stages. In addition to AFRL/VS personnel, system design is by CSA Engineering Inc., and engineering support is provided by Jackson & Tull Inc., and Ohio University. The active gravity off-loading system presented herein, see Figure 1, is designed to deploy in conjunction with a test article while providing constant active load support. The horizontal positioning is to be accomplished with the goal of minimizing the deflection angle of the off-loading cable, connected to points of a deployable space structure, while also minimizing the oscillations added to a test article from cart movement. Load support is to be accomplished with an active system, to reduce the magnitude of mass loading.

Each cart's horizontal movement is provided by a gear drive and each cart suspension is by three freely moving steel wheels, see Figure 1. Also highlighted in Figure 1 are the off-loading tether guide tube and deflection angle sensor. The deflection of the tether is measured by a full-bridge strain gauge sensor, mounted on the bending flexure, allowing the measuring of the angular deflection of the tether and tether guide tube in the ±5° range. The concept for the horizontal positioning, analytical system modeling and subsequent optimal controller development are presented in this paper. Preliminary results from testing of the prototype cart shown in Figure 1, and comparison with the analytical model are presented as well.

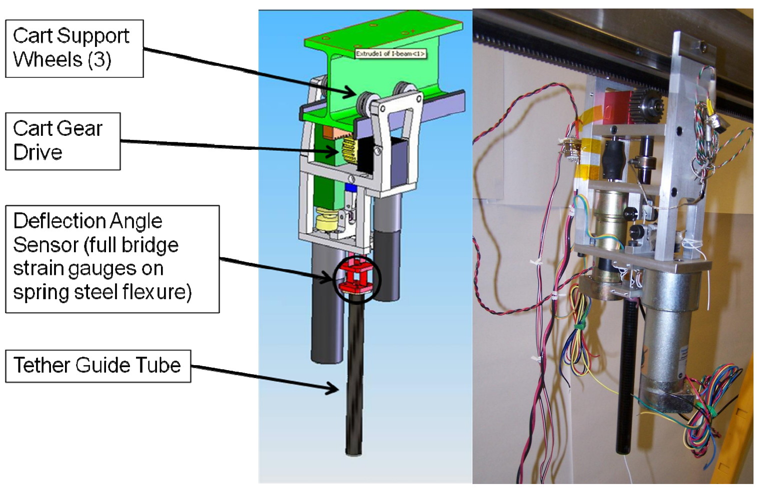

Figure 1, Conceptual and Prototype Active Gravity Off-loading Cart

2. SYSTEM DESCRIPTION AND MODELING

The system under analysis was modeled with respect to the anticipated system dynamics and kinematics, see Figure 2. It is assumed that there will be $i = 1, 2, \ldots n$ carts acting upon the same structure for multiple, n, gravity off-loading points. Coupling between the carts through the test article is anticipated; however, the current system electronics are not planning on incorporating any inter-cart communication ability for design simplicity.

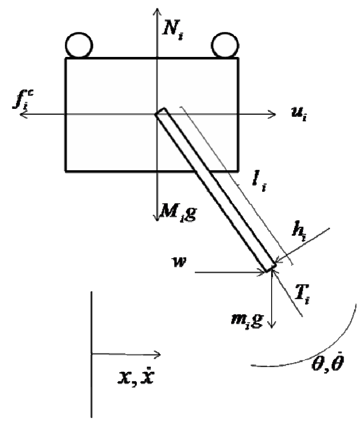

Figure 2, Individual Cart Dynamics and Kinematics

By inspecting Figure 2 the kinematics of the cart are derived as

$$\vec{x}_i = x_i \hat{i} \tag{1a}$$
$$\vec{v}_i = \dot{x}_i \hat{i} \tag{1b}$$
$$\vec{a}_i = \ddot{x}_i \hat{i}. \tag{1c}$$

And the kinematics of the pendulum were derived as

$$\vec{x}_i^{\,p} = (x_i + l_i \sin\theta_i)\hat{i} - l_i \cos\theta_i \hat{j} \tag{2a}$$
$$\vec{v}_i^{\,p} = (\dot{x}_i + l_i \dot{\theta}_i \cos\theta_i)\hat{i} + l_i \dot{\theta}_i \sin\theta_i \hat{j} \tag{2b}$$
$$\vec{a}_i^{\,p} = (\ddot{x}_i + l_i \ddot{\theta}_i \cos\theta_i - l_i \dot{\theta}^2{}_i \sin\theta_i)\hat{i} + (l_i \ddot{\theta}_i \sin\theta_i + l_i \dot{\theta}^2{}_i \cos\theta_i)\hat{j} \tag{2c}$$

where l_i represents the length of the pendulum and θ_i is the angular deflection of the pendulum on a cart.

By inspection, the dynamics acting upon the cart based upon the free-body diagram, Figure 2, yield the following equations of motion

$$\vec{F}_i = F_x^i \hat{i} + F_y^i \hat{j} \tag{3a}$$
$$F_x^i = u_i + T_i \sin\theta_i - f_i^c \dot{x}_i + h_i \theta_i \cos\theta_i \tag{3b}$$
$$F_y^i = N_i - M_i g - T_i \cos\theta_i + h_i \theta_i \sin\theta_i \tag{3c}$$

where, f_i^c is some coefficient of friction acting upon the movement of the cart from both the gear-tooth contact driving the cart and the wheels guiding the cart's motion, h_i is some force due to the spring constant of the spring steel hinge acting upon the rotational movement of the pendulum, g is the acceleration due to gravity and M_i is the mass of the cart assembly.

By inspecting the forces acting upon the pendulum, a set of equations of motion for the pendulum can be derived

$$\vec{F}_i^{\,p} = F_x^p \hat{i} + F_y^p \hat{j} \tag{4a}$$
$$F_x^p = w_i - T_i \sin\theta_i - h_i \theta_i \cos\theta_i \tag{4b}$$

$$F_y^p = -m_i g + T_i \cos\theta_i - h_i\theta_i \sin\theta_i \tag{4c}$$

where m_i is the point mass of the pendulum assembly attached to a uniformly thin bar of length l_i.

It is assumed that the cross-product of the length of the pendulum and the force due to the spring constant of the spring steel hinge results is a $\hat{k}$ -component force from the i^{th} pendulum hinge through

$$\begin{aligned} \vec{l}_i \cdot \vec{h}_i &= l_i \cdot h_i \sin \pi/2 = l_i \cdot h_i \\ &\widehat{=} \kappa_i^p \cdot \theta_i \end{aligned} \tag{5}$$

where κ_i^p is the i^{th} pendulum hinge resistance to bending. However, in this case it is expected that there is a spring force acting upon the hinge due to simultaneous translation and deflection of the beam, causing different types of geometric deflections to occur simultaneously, behaving as both a cantilevered beam and bending from the torsion of a clamped-pinned beam [6]-[8]. However, only the bending of the hinge behaving as the torsion of a clamped-pinned beam was considered; this is due to the analysis being an approximation of the system with higher order effects ignored. Therefore, the force from the spring constant of the pendulum's hinge are represented through

$$\kappa_i^p \theta_i = \frac{\kappa_i^p}{l_i}\theta_i. \tag{6}$$

Applying Newton's 2nd law to the cart and pendulum system yields the equations of motion

$$u_i + T_i \sin\theta_i - f_i^c \dot{x}_i + h_i\theta_i \cos\theta_i = M_i \ddot{x}_i \tag{7a}$$

$$N_i - M_i g - T_i \cos\theta_i + h_i\theta_i \sin\theta_i = 0 \tag{7b}$$

$$w_i - T_i \sin\theta_i - h_i\theta_i \cos\theta_i = m_i\left(\ddot{x}_i + l_i\ddot{\theta}_i \cos\theta_i - l_i\dot{\theta}^2{}_i \sin\theta_i\right) \tag{7c}$$

$$-m_i g + T_i \cos\theta_i - h_i\theta_i \sin\theta_i = m_i\left(l_i\ddot{\theta}_i \sin\theta_i + l_i\dot{\theta}^2{}_i \cos\theta_i\right) \tag{7d}$$

The equations of motion describing the system can then be reduced to

$$\ddot{x}_i = \frac{1}{M_i + m_i \sin^2\theta_i}\begin{pmatrix} h_i\theta_i \cos\theta_i + m_i g \sin\theta_i \cos\theta_i \\ + m_i l_i \dot{\theta}_i^2 \sin\theta_i - f_i^c \dot{x}_i + u_i + w_i \sin^2\theta_i \end{pmatrix} \tag{8a}$$

$$\ddot{\theta}_i = \frac{1}{l_i\left(M_i + m_i \sin^2\theta_i\right)}\begin{pmatrix} -\left(m_i + M_i\right) g \sin\theta_i - m_i l_i \dot{\theta}_i^2 \sin\theta_i \cos\theta_i \\ + f_i^c \dot{x}_i \cos\theta_i - \left(1 + \dfrac{M_i}{m_i}\right) h_i\theta - u_i \cos\theta_i + \dfrac{M_i}{m_i} w_i \cos\theta_i \end{pmatrix}. \tag{8b}$$

To create a set of linearized differential equations, θ is assumed to be in the range of $-5° \leq \theta \leq 5°$ with positive angles in the counter clockwise direction. This is the same range that the circuitry of the flexure angle sensor will provide, allowing this to be a reasonable linearization. Applying small angle approximation

$$\sin\theta_i \approx \theta_i \tag{9a}$$

$$\cos\theta_i \approx 1 \tag{9b}$$

$$\theta_i^2 \approx 0 \tag{9c}$$

$$\dot{\theta}_i^2 \approx 0 \tag{9d}$$

for the system results in the following set of equations

$$\ddot{x}_i = \frac{h_i}{M_i}\theta_i + \frac{m_i g}{M_i}\theta_i - \frac{f_i^c}{M_i}\dot{x}_i + \frac{1}{M_i}u_i \tag{10a}$$

$$\ddot{\theta}_i = -\frac{h_i}{m_i l_i}\left(1+\frac{m_i}{M_i}\right)\theta_i - \frac{g}{l_i}\left(1+\frac{m_i}{M_i}\right)\theta_i + \frac{f_i^c}{M_i l_i}\dot{x}_i - \frac{u_i}{M_i l_i} + \frac{1}{m_i l_i}w_i. \tag{10b}$$

Simplifying the above equations of motion by substituting the pendulum hinge spring constant equation yields

$$\ddot{x}_i = \frac{\kappa_i^p}{M_i l_i}\theta_i + \frac{m_i g}{M_i}\theta_i - \frac{f_i^c}{M_i}\dot{x}_i + \frac{1}{M_i}u_i \tag{11a}$$

$$\ddot{\theta}_i = -\frac{\kappa_i^p}{m_i l_i^2}\left(1+\frac{m_i}{M_i}\right)\theta_i - \frac{g}{l_i}\left(1+\frac{m_i}{M_i}\right)\theta_i + \frac{f_i^c}{M_i l_i}\dot{x}_i - \frac{u_i}{M_i l_i} + \frac{1}{m_i l_i}w_i. \tag{11b}$$

The state space representation of the system was derived to take into account disturbances to the system and all perceivable dynamics involved

$$\dot{z}_i = Az_i + Bu_i + B_w w_i \tag{12}$$

where $z_i \in \Re^4, u_i \in \Re^4$ and $w_i \in \Re^4$ are the state, input and disturbance vectors. The state space representation of the gravity off-loading system dynamics and kinematics were found to be

$$A = \begin{bmatrix} 0 & 1 & 0 & 0 \\ 0 & -\frac{f_i^c}{M_i} & \frac{m_i g}{M_i} + \frac{\kappa_i^p}{M_i l_i} & 0 \\ 0 & 0 & 0 & 1 \\ 0 & \frac{f_i^c}{M_i l_i} & -\left(\frac{g}{l_i} + \frac{\kappa_i^p}{M_i l_i^2}\right)\left(1+\frac{m_i}{M_i}\right) & 0 \end{bmatrix} \quad B = \begin{bmatrix} 0 \\ \frac{1}{M_i} \\ 0 \\ -\frac{1}{M_i l_i} \end{bmatrix} B_w = \begin{bmatrix} 0 \\ 0 \\ 0 \\ \frac{1}{m_i l_i} \end{bmatrix} \tag{13}$$

with the state vector assumed to be representative of the translational position and translational velocity of the cart and the angular position and angular velocity of the pendulum, or

$$z_i = \begin{bmatrix} x_i & \dot{x}_i & \theta_i & \dot{\theta}_i \end{bmatrix}^T. \tag{14}$$

3. LINEAR QUADRATIC GAUSSIAN CONTROLLER EQUATIONS

A linear quadratic Gaussian (LQG) controller was developed due to the anticipation of random disturbance inputs on the flexure. LQG controllers are designed to take disturbances into account and LQG controllers do not assume that all states are known at all times. This is accomplished by designing a controller that consists of an optimal state feedback gain, in this case a linear quadratic regulator (LQR) gain, and a Kalman filter, for an optimal observer [9]. This gives the LQG controller more versatility when controlling a system that has various random disturbances, such as the system under consideration here, than other optimal controllers such as the LQR would have. In this analysis the LQG controller was created through calculating the LQR compensator, calculating the Kalman filter gains and then combining the two to create an LQG compensator [9].

An LQG controller assumes that the system being controlled has a general form

$$\dot{x} = Ax + Bu + Dw \tag{19a}$$

$$y = Cx + Du + Hw + v \tag{19b}$$

where w is assumed to be a Gaussian random disturbance input and v is assumed to be some random disturbance in the measurement [9]. The LQR regulator gain matrix, K, component of the compensator is determined for

$$u = -Kx \tag{20}$$

so that the quadratic cost function

$$J_N = \int_0^\infty \left(x^T Qx + u^T Ru\right)dt \tag{21}$$

can be minimized, with Q being a positive semi-definite state weighting matrix and R being a positive definite control effort penalizing matrix [9]. The weighting matrices determined through the minimum solution to the quadratic cost function were found by solving the Algebraic Riccati Equation for the matrix P

$$A^T P + PA - PBR^{-1}B^T P + Q = 0 \tag{22}$$

where P is assumed to be the positive definite [9]. The LQR gain is then calculated via the method from [9]

$$K = R^{-1}B^T P \tag{23}$$

providing the weighting matrices for the state effort, Q, and input effort, R, are chosen through using discretion and balancing the tradeoffs between the inputs.

To create the LQG compensator, a Kalman filter is needed to create the optimal observer part of the compensator [9]. Due to the presence of random disturbances, an estimated state equation will be used for deriving the Kalman filter portion of the compensator. The estimated state equations is therefore represented by

$$\dot{\hat{x}} = (A - LC)\hat{x} + Bu + Ly. \tag{24}$$

Substituting in the output state equation yields

$$\dot{\hat{x}} = A\hat{x} + Bu + L(y - C\hat{x} - Du). \tag{25}$$

The optimal LQG feedback controller can then be obtained by substituting the estimated state $\hat{x}$ for the state feedback controller design u=-Kx. Substituting the result into the estimated state equation results in

$$\dot{\hat{x}} = A\hat{x} + BK\hat{x} - LC\hat{x} + LDK\hat{x} + Ly. \tag{26}$$

Grouping terms together yields

$$\dot{\hat{x}} = (A - BK - LC + LDK)\hat{x} + Ly. \tag{27}$$

By inspection, the LQG state matrix is defined as $A_e = [A - BK - LC + LDK]$, the input matrix is defined as $B_e=L$. The output matrix is defined as $C_e=-K$, and the feedthrough matrix is defined as $D_e=[zeros(size(K),N)]$ [9].

4. SIMULATIONS AND RESULTS

4.1 Analytical Cart Simulation Results

To analyze the natural behavior of the system a simulation of the behavior of the cart to a random initial deflection angle of the flexure was considered, see Figure 3. The random deflection angle was considered as a Gaussian random distributed input, with a mean of zero, a variance of one, and a standard deviation of one. The result of this analysis indicates that the cart enters a limit cycle in the absence of control from the marginal stability of the system, from the presence of a pole at the origin [10], see Table 1.

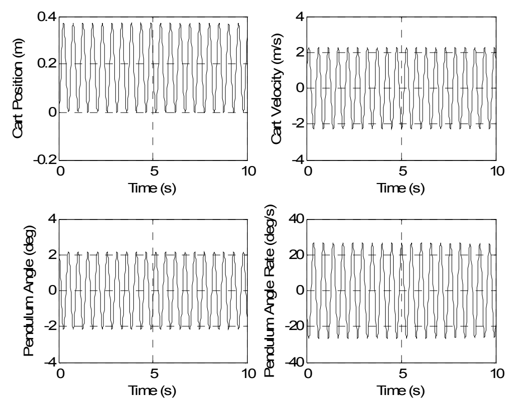

Figure 3, Open Loop Response to a Random Initial Flexure Angle

Table 1, Eigenvalues of the Uncompensated System

0
$-0.0008 \pm 12.1699i$
-0.0012

Simulations involving the closed loop response of the compensated system were first analyzed with regard to the same initial conditions as used in the uncompensated case, Figure 4. By inspection the pendulum angle converges to zero following the deflection, and the system's stability has been greatly improved. Responses are well within the desired pendulum angle range of ±5°.

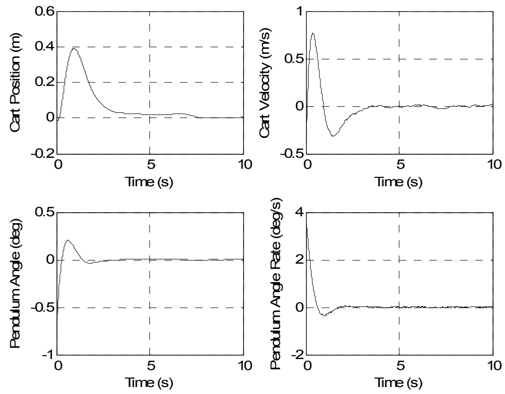

Figure 4, LQG Compensated Response to Random Initial Conditions

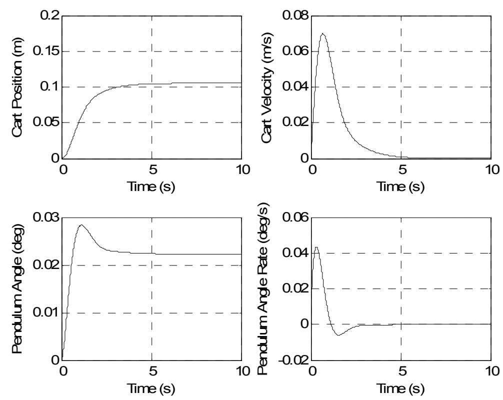

Figure 5, LQG Compensated System Response to a Unit Step Input

The step response of the LQG compensated system is shown in Figure 5. The response of the system is consistent with the system response to a random initial deflection angle and again well within the desired range. The stability of the system can be verified by observing the eigenvalues of the observer, see Table 2, and the eigenvalues of the LQG compensated system, see Table 3. Both tables show no positive real eigenvalues; additionally, the eigenvalues of the LQG compensated system have moved further negative in magnitude than in the uncompensated case, Table 1, confirming the system's closed loop stability.

Table 2, Eigenvalues of the LQG Observer

-2739.4	-5.4
-42.1	-2.2

Table 3, Closed Loop Eigenvalues of the LQG Compensated System

-1292.6	-1	$-2.1\pm2.5i$
-186.7	-1	$-2.5\pm2.3i$

4.2 Prototype Cart Results

The prototype cart, Figure 1, was fabricated in 1st Quarter Fiscal Year 2007 after analyzing the behavior of the horizontal positioning of the conceptual model. The preliminary results of the horizontal positioning of the prototype indicated a natural behavior similar to that of the analytical model. Currently, electronics for all sensors on the prototype have not been fabricated, the sensor flexure position being the only one available at this time, and therefore only knowledge about θ from (14) was known. Without knowledge of the cart position, it was impossible to implement the optimal control scheme above. This resulted in the development of a single-input-single-output (SISO) proportional-plus-integrator (PI) controller being developed for proof of concept testing with flexure position as the input and the pulse width modulation (PWM) duty cycle of the horizontal position motor as the output.

Testing the SISO PI controlled prototype cart after a disturbance input of approximately 3° was applied to the flexure, Figure 6, produced results similar to the natural behavior of the cart from a random input, Figure 3. However, by observing the behavior of the cart, it was determined that the magnitude of static friction experienced by the cart and the spring constant of the flexure were both higher than previously estimated. This resulted in the cart overshooting both the desired flexure angular position and the ±5° flexure sensor range, causing the cart to exhibit the oscillatory behavior seen in Figure 6.

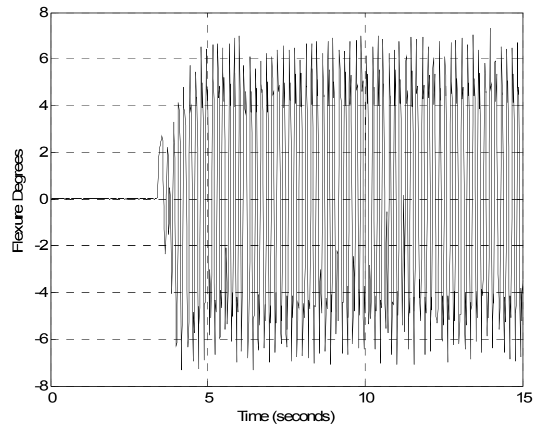

Figure 6, PI Compensated Prototype System Response to a Disturbance Input

Foam dampers were added to the prototype's flexure to solve these problems with the outcome being a cart that can track a disturbance input to the flexure, Figure 7, with a settling time of approximately 0.75 seconds. This is similar in magnitude of the settling time of the LQG controlled system, Figure 5; however, it should also be noted that the response of the cart with the SISO PI controller is significantly not as smooth as that provided by the optimal controller.

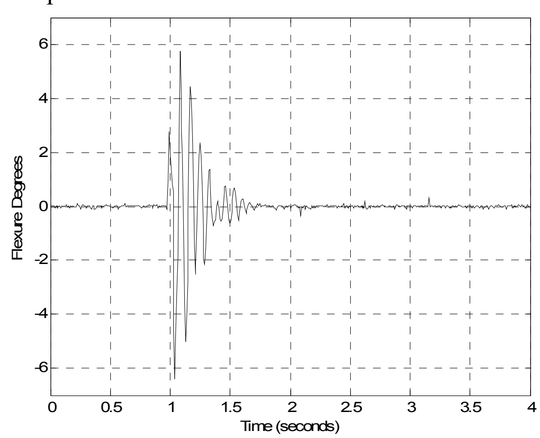

Figure 7, Damped PI Compensated Prototype Response to Disturbance Input

5. CONCLUSIONS

The system modeling, controller design, and verification for the horizontal positioning of a proposed active gravity off-loading system was presented. The system modeling took into account all anticipated dynamics and kinematics components in the gravity off-loading cart. The analysis of the model included situations that are consistent with the expected operating environment, such as introducing a random deflection of the flexure and introducing a step input to the system. The result of this analysis shows a system that is marginally stable and will fall into a limit cycle in the absence of a controller. With the presented optimal control scheme, the system is able to meet the requirement of keeping the flexure deflection angle to within ±5°.

Comparisons with the preliminary results from the horizontal positioning controller of the prototype cart were presented as well. Although the controller used on the prototype was a PI controller instead of an optimal controller, comparisons on the behavior of the cart could be made. Also of note is that the electronics currently used on the prototype cart do not permit measurement of flexure angles outside a ±5° range and have a resolution of only 0.1°. This deviates significantly with the assumptions made in the analytical model, where full knowledge of the state variables was assumed. However, even with the PI controller, the cart was still controllable to within the ±5° range, but the response was not as smooth as with the conceptual optimal controller. When positioning sensor fabrication has been completed, the conceptual controller can be applied to the prototype for full system testing.

ACKNOWLEDGEMENTS

The authors would like to express their gratitude to the many people who supported the work herein, including A. Biskner, CSA Engineering Inc., for cart design and fabrication, G. Sanford, CSA Engineering Inc., for engineering support, H. P. Dumm, Jackson and Tull Inc., for cart power system design and engineering support, N. Martz, Jackson and Tull Inc., for electronics fabrication, and W. Manning, Applied Technology Associates, for embedded controller troubleshooting.

REFERENCES

[1] T. Murphey, "Booms and Trusses," *Recent Advances in Gossamer Spacecraft (Progress in Astronautics and Aeronautics).* Ed. Christopher H. M. Jenkins, American Institute of Aeronautics and Astronautics, Jan. 30, 2006, pp. 1-43.

[2] M. D. Griffin and J. R. French, *Space Vehicle Design*, American Institute of Aeronautics and Astronautics, Inc., Washington, DC, 1991, pp. 348-349.

[3] D. A. Kienholz, "CSA Pneumatic/Magnetic Suspension System Application Note No. 2: Comparison to Buoyancy Devices (Helium Balloons)," *Prepared for Sandia National Laboratories*, CSA Engineering Inc., Palo Alto, CA, May 1993.

[4] J. W. Stokes, E. E. Engler and W. E. Agan, "Neutral Buoyancy Test Results of a Deployable Space Beam," *2nd AIAA Conf. on Large Space Platforms*, San Diego, CA, Feb. 2-4, 1981.

[5] A. C. Biskner, Mechanical Engineer, CSA Engineering, personal communication, 5 July 2006.

[6] E. Ardelean, Mechanical Engineer, Science Applications International Corporation, personal communication, 2 August 2006.

[7] R. D. Blevins, *Formulas for Natural Frequency and Mode Shape*, Krieger Publishing Company, 2001 (pp. 39-47)

[8] A. Cretu, *Rezistenta Materialelor cu elemente de Elasticitate si de Plasticitate*, Universitatea Tehnicǎ din Cluj-Napoca, 1993 (pp. 147)

[9] J. Mitchell, "Lecture notes on digital control systems," Ohio University, Winter – Spring Quarters, Academic Year 2005-2006.

[10] L. Perko, *Differential Equations and Dynamical Systems*, 2nd Edition, Springer, 1996.